



Cite this: *Nanoscale*, 2018, **10**, 21335

Adsorption and diffusion of lithium polysulfides over blue phosphorene for Li–S batteries†

Sankha Mukherjee,^a Lance Kavalsky,^a Kinnor Chattopadhyay^{a,b} and Chandra Veer Singh^{*a,b}

Lithium–sulphur (Li–S) batteries suffer from capacity loss due to the dissolution of lithium polysulfides (LiPSs). Although finding cathodes that can trap LiPSs strongly is a possible solution to suppress the “shuttle” effect, fast diffusion of lithium and LiPSs is also pivotal to prevent agglomeration. We report that monolayer blue phosphorene (BP), a recently synthesized two-dimensional material, possesses these characteristics as a cathode in Li–S batteries. Density functional theory calculations showed that while the adsorption energies (E_b) of various LiPSs over pristine BP are reasonably strong (from -0.86 eV to -2.45 eV), defect engineering of the lattice by introducing a single vacancy (SV) increased the binding strength significantly, with E_b in the range of -1.41 eV to -4.34 eV. *Ab-initio* molecular dynamics simulations carried out at 300 K showed that the single vacancies trap the Li atoms in the LiPSs compared to pristine BP. Projected density of states revealed that the creation of an SV induces metallicity in the cathode. Furthermore, an increase in the adsorption strength did not cause significant structural deformation, implying that the soluble large LiPSs did not decompose, which is essential to suppress capacity fading. The energy barriers for LiPSs’ migration over pristine BP are minimal to ensure ultrafast diffusion, with the lowest diffusion energy barriers being 0.23 eV, 0.13 eV and 0.18 eV for Li_2S_4 , Li_2S_6 and Li_2S_8 , respectively. Furthermore, the energy barrier associated with the catalytic oxidation of Li_2S over pristine and defective BP was found to be greater than three times smaller compared to graphene, which suggests that charging processes could be faster by orders of magnitude. Therefore, BP with a suitable combination of defects would be an excellent cathode material in Li–S batteries.

Received 14th June 2018,
Accepted 3rd October 2018
DOI: 10.1039/c8nr04868a
rsc.li/nanoscale

Introduction

Lithium–sulfur (Li–S) batteries are a viable option for large-scale rechargeable energy-storage systems because they are cheap, render high energy density and are less toxic than current offerings.^{1–4} However, there are several challenges which currently limit their large-scale commercialization, for example, capacity fading and moderate cycle performance, poor stability of the anode, and active material loss in the cathode.⁵ In a Li–S battery during discharge, the Li^+ ions migrate from the anode to the cathode and reduce the cyclooctasulfur (S_8) molecules residing in the cathode to form polar lithium polysulfides (Li_2S_x , $1 \leq x \leq 8$). These resulting polysulfides can be either soluble ($3 \leq x \leq 8$) or insoluble ($x = 1, 2$) in the liquid electrolyte. Because of the formation of these dis-

charge products, the cathode undergoes several compositional and structural alterations causing mechanical disintegration and critical capacity fading. Furthermore, the sulfur containing carbonaceous cathodes are poor binders of the soluble polysulfides.⁵ Consequently, during discharge, these soluble polysulfides get dissolved in the electrolyte and migrate to the anode, resulting in redeposition, thereby constructing a passivation layer, a phenomenon commonly known as the shuttle effect.^{3,6} These side-reactions result in a low coulombic efficiency and a short life.⁶ Additionally, the carbonaceous cathode and the final discharge product (Li_2S) both act as insulators, causing passivation of the cathode for electrochemical reactions.

Over the past decade, efforts have been made to address some of these issues in the large-scale commercial realization of Li–S cells. Recently, Lee *et al.*⁷ showed that while electrolytes such as $\text{ACN}_2\text{LiTFSI}$ permit the migration of Li^+ ions, they inhibit the shuttle effect by selectively suppressing the dissolution of LiPSs. On the cathode side, hollow carbon spheres of sulfur containing composites, nanoporous carbon, and carbon nanofibers were attempted to bind the lithium polysulfides (LiPSs) on the cathodic host.⁸ In general, an ideal catho-

^aDepartment of Materials Science and Engineering, University of Toronto, Toronto, Ontario M5S 3E4, Canada. E-mail: chandraveer.singh@utoronto.ca

^bDepartment of Mechanical and Industrial Engineering, University of Toronto, 5 King’s College Road, Toronto M5S 3G8, Canada

†Electronic supplementary information (ESI) available. See DOI: 10.1039/c8nr04868a

die host should be a conductive material and be able to strongly adsorb lithium polysulfides (the binding energies of Li_2S_x species on the anchoring should be greater in magnitude than 0.8 eV) to avoid their dissolution in the electrolyte, thereby inhibiting the shuttle effect.⁹ Additionally, the cathodic material should allow ultrafast diffusion of ions and LiPSs to promote conversion of adsorbed large LiPSs to insoluble $\text{Li}_2\text{S}_2/\text{Li}_2\text{S}$ and attain efficient Sulfur utilization.¹⁰ In this context, the emergence of two dimensional (2D) materials is significant due to their unique structural (a large electrochemical active surface and a large number of adsorption sites for uniform adsorption of LiPSs and deposition of $\text{Li}_2\text{S}_2/\text{Li}_2\text{S}$), and electrical and mechanical properties. Recently, it has been shown that the incorporation of 2D materials (graphene,¹¹ ReS_2 ,¹² Ti_3C_2 and $\text{Ti}_3\text{CN}^{13}$) into the cathode matrix can significantly improve the performance of Li-S batteries. For example, Li *et al.* demonstrated that Li-S cells utilizing black phosphorene possess a capacity of 660 mA h g^{-1} with only 0.053% capacity fade, whereas those without it show 0.25% capacity fade after 200 cycles; DFT simulations indicated that this improvement in performance was due to the stronger interaction between black phosphorene and the polysulfides.¹⁴ These experimental studies have inspired theorists to study several other 2D materials for their potential use as a component in the cathodes for Li-S batteries.^{15–19} However, much remains unexplored due to the rapidly growing catalogue of 2D materials. For example, theoretical calculations have so far predicted more than 21 two-dimensional polymorphs for phosphorus, commonly known as phosphorene. Blue phosphorene, another 2D polymorph of P, was first theoretically predicted in 2014,²⁰ followed by its successful synthesis using molecular beam epitaxy^{21,22} and has a puckered surface similar to the structure of silicene and germanene. First principles investigations have studied the suitability of monolayer BP for alkali-metal-ion batteries,²³ and BP/graphene, BP/ NbS_2 and BP/ TaS_2 ²⁴ heterostructures as electrodes in lithium-ion batteries. Based on these theoretical estimates, the applicability of pristine monolayer BP as a cathode in Li-S batteries is worth exploring.

Attempts have been made to modify the electronic properties of 2D materials for increasing their interaction strength with the LiPSs, such as heteroatom doping and defect engineering. For example, it was demonstrated using both experiments and first principles based simulations that N-doped graphene with pyrrolic and pyridinic N-dopants bind polysulfides more strongly than pristine graphene.^{25,26} Additionally, amino-functionalized reduced graphene oxide²⁷ and lithium trapped N-doped graphene²⁸ have also been reported to possess strong interactions with the LiPSs. Similarly, crystallographic defects (such as point defects and grain boundaries), which are formed during the synthesis of 2D materials from their bulk structures using deposition techniques or exfoliation, can significantly alter the electronic properties of the material. Yet, our understanding of how different crystallographic defects in 2D materials affect the performance of Li-S batteries is incomplete. So far, the lion's share of the efforts has been dedicated towards understanding the effect of defects on the perform-

ance of Li-S batteries containing graphene as the cathode.^{29–31} For example, Zhao *et al.*³⁰ have predicted that defective graphene helps to trap S due to the electronic and geometric effects. They also suggest that defects can help distribute S atoms uniformly over the cathode, and in effect reduce the chemical activity of S. Furthermore, Jand *et al.*³¹ reported that due to the strong interactions between defective graphene and polysulfides, one S atom is detached from the polysulfide molecule, forming a $\text{Li}_2\text{S}_{x-1}$ molecule, which binds softly over the S-doped graphene host. On the other hand, a recent article by Jiang *et al.* reported that defective borophene reduces the adsorption strength of LiPSs compared to pristine borophene and suppresses the decomposition of LiPSs.³² Questions such as whether BP with defects can trap polysulfides and what are the underlying mechanisms of interactions remain unanswered.

To determine monolayer pristine and defective BP's capability to serve as a cathode in Li-S batteries, we investigated the adsorption of various LiPSs on BP using extensive density functional theory calculations. First, favorable sites for the adsorption of the LiPSs over pristine BP were determined. To study the effect of defects on LiPS binding, monolayer BP with a single vacancy was investigated. In addition, Climbing Image-Nudged Elastic Band (CI-NEB) simulations were employed to determine the minimum energy pathways and the diffusion energy barriers for the transport of Li atoms and polysulfides over pristine BP. The results presented in this study demonstrate that monolayer BP is well suited as a positive electrode for next-generation Li-S batteries.

Computational details

Plane-wave based density functional theory calculations were performed using the Quantum Espresso³³ software package. The projector augmented wave (PAW) method³ with the Perdew–Burke–Ernzerhof (PBE) formulation was used to capture the interactions between valence electrons and the ionic cores, and approximate the exchange correlation term, respectively. The structure of BP was obtained using a kinetic energy cutoff of 70 Ry ($\sim 952 \text{ eV}$) for the wave functions and 350 Ry ($\sim 4761 \text{ eV}$) for the charge densities, respectively. A vacuum of 20 \AA was used to eliminate spurious interlayer interactions due to periodicity, and the convergence criterion for the self-consistent field was set at 1×10^{-6} Ry. The primitive cell of free-standing monolayer BP was obtained using a Broyden–Fletcher–Goldfarb–Shanno algorithm³⁴ over a $13 \times 13 \times 1$ Monkhorst–Pack grid of k -points with the residual Hellmann–Feynman force on each atom of less than $0.0001 \text{ Ry per Bohr}$, and the total energy converged of less than 5×10^{-5} Ry. A $4 \times 4 \times 1$ Monkhorst–Pack grid of k -points was used for optimizing the structure of the pristine BP supercell which contained 5×5 primitive cells (with 50 atoms) and the adsorption energy. The DFT-D2 approach³⁵ was utilized to accurately account for long-range van der Waals (vdw) forces. Bader charge analysis³⁶ was performed to quantify the charge trans-

fer process during LiPS adsorption. Additionally, the binding energy (E_b) and charge density difference (ρ_b) were determined using

$$E_b = E_{\text{Adsorbedstate}} - (E_{\text{Adsorbent}} + E_{\text{BP}}), \quad (1)$$

$$\rho_b = \rho_{\text{Adsorbedstate}} - (\rho_{\text{Adsorbent}} + \rho_{\text{BP}}), \quad (2)$$

where $E_{\text{Adsorbedstate}}$ is the energy of BP after the adsorption of LiPSs, $E_{\text{Adsorbent}}$ is the energy of isolated LiPS molecules, and E_{BP} is the energy of pristine and defective BP. A negative E_b indicates that the adsorption of the LiPSs is energetically favored. Similarly, $\rho_{\text{Adsorbedstate}}$ is the charge density of BP after the adsorption of the LiPSs, $\rho_{\text{Adsorbent}}$ is the charge density of isolated LiPS molecules, and $\rho_{\text{Substrate}}$ is the charge density of pristine and defective BP. Variable-cell *ab initio* molecular dynamics (AIMD) simulations were utilized to assess the thermodynamic stability of the BP primitive cell. For the AIMD calculations, a velocity rescaling scheme was utilized to keep the temperature at 300 K with a time step of 2 fs for relaxation. The climbing image nudged elastic band (CI-NEB) method was used to obtain estimates of energy barriers for the diffusion of Li and LiPSs over BP.³⁷

Results and discussion

Structural properties of the reactants

The relaxed structure of the monolayer BP supercell used for the calculations is shown in Fig. 1a; the primitive cell is shown using pink lines. The lattice constants of the primitive cell were found to be $a_1 = a_2 = 3.28 \text{ \AA}$, which agrees well with previous reports (3.28 \AA (ref. 38) and 3.268 \AA (ref. 24)). In BP, each P atom is covalently bonded to three P neighbors, with a P–P bond length of 2.26 \AA and a bond angle of 93° . A single P atom was removed from the BP supercell and the structure was optimized in the ground state to obtain the defective structure (Fig. 1b). AIMD simulations were performed to assess the thermodynamic stability of the single vacancy (SV) supercell at 300 K and the time traces of temperature and potential energy are shown in Fig. 1c. The formation energy of a single vacancy in blue phosphorene (SVBP) is given by the equation:

$$E_f = E_{\text{defect}} - \frac{N - i}{N} E_{\text{pristine}} \quad (3)$$

where E_{defect} and E_{pristine} are the total energies of the defective and pristine BP supercells, respectively, N is the number of P atoms in the pristine supercell, and i is the number of P atoms removed from the pristine supercell to create the defect. The formation energy of a SV in BP in the ground state was 2.42 eV , which is 0.79 eV smaller than that in silicene³⁹ and 5.08 eV smaller than that in graphene.⁴⁰ The areal density of a certain defect at finite a temperature T is related to its formation energy by an Arrhenius type equation given by

$$N_{\text{defect}} = N_{\text{pristine}} \exp\left(-\frac{E_f}{k_B T}\right) \quad (4)$$

where N_{pristine} is the areal density of atoms in the pristine material, and k_B is the Boltzmann constant. The areal densities, N_{pristine} , for graphene and silicene in the ground state are $3.79 \times 10^{19} \text{ m}^{-2}$ and $1.55 \times 10^{19} \text{ m}^{-2}$, respectively.⁴¹ The temperature dependent areal densities of the most stable single vacancy defects in BP, graphene and silicene are shown in Fig. 1d. It can be seen that the areal density of SV at any temperature is orders of magnitude higher in BP as compared to silicene and graphene.

As shown by the PDOS plot in Fig. 1e, pristine BP is a semiconductor material with a band gap of approximately 1.95 eV . However, by the introduction of a single vacancy into the lattice, this picture changes as shown in Fig. 1f with the states being found within the band gap around the Fermi energy. At first, this may seem counterintuitive since the impression is given of states being added from the removal of an atom. However, the cause of this change becomes clearer considering that electrons originally participating in bonds are now dangling and must be in a higher energy state relative to the rest of the valence band.

Adsorption of Li_2S_x on pristine and defective blue phosphorene

In Li–S batteries the Li^+ ions migrate from the anode, through the electrolyte and interact with the sulphur-containing cathode to form various lithium polysulfide intermediates during discharge. As shown in Fig. 1a, the surface of pristine BP possesses four structurally unique adsorption sites, which are: (i) a C-site above the center of the P-hexagon, (ii) an R-site above a P atom in the ridge, (iii) a B-site above the center of a P–P bond, and (iv) above the P atom along the pucker (P-site). A set of distinct translational and rotational configurations of the LiPSs were considered over these high-symmetry sites in pristine BP to find the most energetically favorable binding site. As an example, various configurations of Li_2S_6 molecules tested here are shown in Fig. 2(a–k). The adsorption energies of Li_2S_6 for all these configurations are not identical, as shown in Fig. 2(l), which demonstrates the need to search for the optimal arrangement. The same method was utilized to find the most energetically stable adsorption configurations of the remaining Li polysulfides and S_8 . The most stable adsorption configurations of all the Li polysulfides and S_8 versus the corresponding values of E_b are displayed in Fig. 3. Additionally, some key structural parameters are presented in Table 1. It can be seen that the interaction strength of S_8 and the polysulfides over pristine BP are reasonably strong, with the strongest adsorption energies being -0.51 eV for S_8 , -0.95 eV for Li_2S_8 , -0.86 eV for Li_2S_6 , -1.07 eV for Li_2S_4 , -1.16 eV for Li_2S_3 , -1.54 eV for Li_2S_2 , and -2.46 eV for Li_2S . These adsorption energies are much larger than that of pristine graphene²⁵ and are comparable to that of black phosphorene.⁴² The energy gain associated with the cluster formation of Li_2S_x is significantly smaller than the adsorption energies of the LiPSs over BP. For example, the energy increase associated with the formation of soluble LiPSs, *i.e.* Li_2S_8 , Li_2S_6 , and Li_2S_4 networks, are 0.54 eV , 0.6 eV , 0.8 eV (ref. 43), which are much

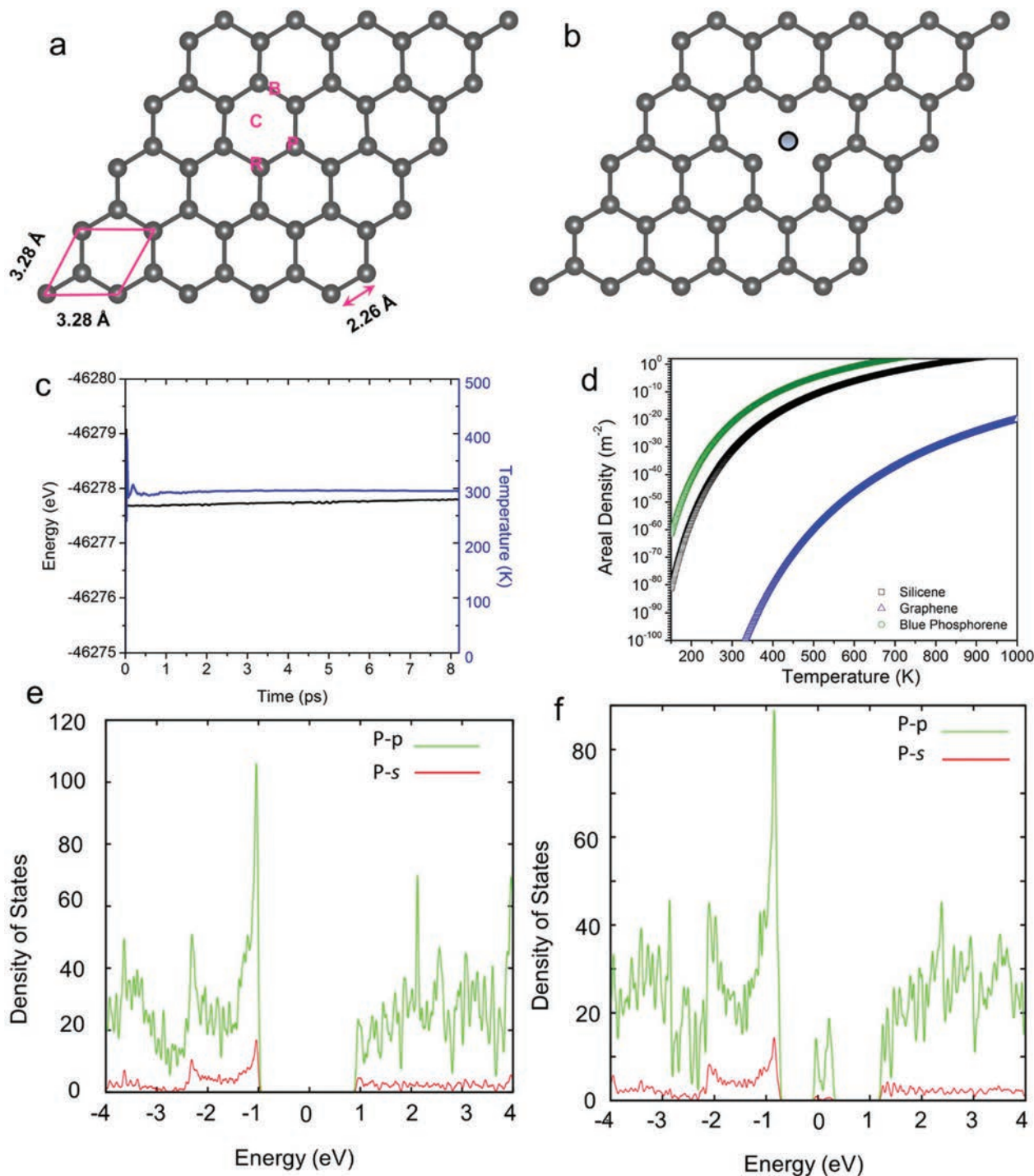


Fig. 1 (a) Top view of pristine BP; the primitive cell of BP is shown by a pink rhombus. (b) Top view of single vacancy BP. The hollow circle represents the P atom removed from the pristine supercell to create the single vacancy. (c) Time traces of total energy and temperature of pristine BP obtained using variable cell AIMD simulations. (d) Areal densities of single vacancies in graphene, silicene and BP as a function of temperature. Electronic projected density of states of (e) pristine and (f) SV BP.

smaller than their E_b values over BP. Therefore, these LiPSs would prefer to spread over the BP surface than form networks.

Furthermore, the adsorption energy of S_8 is smaller than that of the LiPSs due to the absence of Li atoms that interact

with the substrate. Additionally, an increase in binding energy with decreasing S content indicates that the discharge process over BP is favorable. Considering the most energetically favorable position, the cyclooctasulfur molecule orients itself parallel to the BP surface at a distance of 3.63 Å; this behavior is

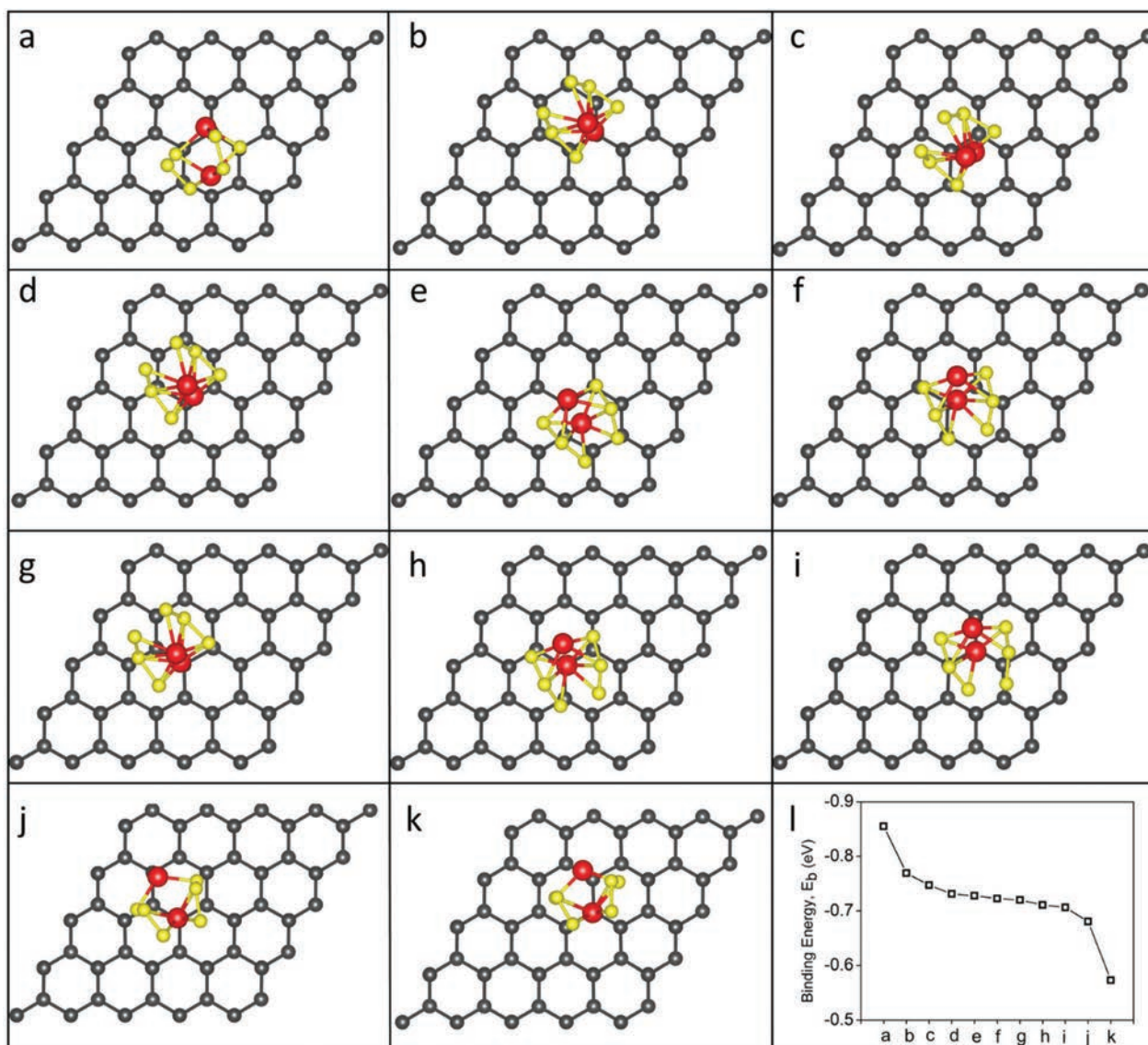


Fig. 2 (a)–(k) Top views of various configurations of Li₂S₆ molecules over monolayer pristine blue phosphorene. (l) Binding energy of Li₂S₆ on the blue phosphorene for each arrangement.

similar to black phosphorene,⁴² N-doped and amorphous graphene,^{9,28} C₃B,⁴⁴ and Ti₂CO₂.⁴⁵ Similarly, the Li atoms in LiPSs are located near the BP surface (except for Li₂S and Li₂S₆) while the S atoms are located away from it. A previous study reported that the C-site and the P-site are the most energetically favored locations for the adsorption of Na and K over BP.⁴⁶ Interestingly, the Li atoms in LiPSs are also located near these two sites.⁴⁶ Also, the length of the shortest Li–P bond increases with increasing concentration of S in the LiPSs, because S is highly electronegative. This behavior is similar to that of black phosphorene⁴² and unlike β₁₂ borophene.⁴⁷ Furthermore, we analyzed the lengths of the Li–S bonds in different LiPSs after their adsorption over BP, which revealed that the Li–S bond lengths increased monotonically during adsorption. For example, compared to an isolated Li₂S₈ mole-

cule, the length of the Li–S bond in Li₂S₈ increased by 0.025 Å (Δ_{Li–S}) after its adsorption over pristine BP. Similarly, for Li₂S₄, Li₂S₃, Li₂S₂ and Li₂S molecules after adsorption the Li–S bond lengths increased by 0.028 Å, 0.06 Å, 0.11 Å and 0.34 Å, respectively. The extension of the Li–S bond lengths during the discharge process is an indication of increased interaction between BP and the LiPSs, which is also in agreement with the magnitudes of E_b. The increase in bond length increases with an increase in the Li:S ratio because of strong electronegativity of S compared to the electronegativities of P and Li. In order to obtain insights into the bonding mechanism, we calculated the Bader partial charges³⁶ and differential charge densities (DCD) of Li₂S_x (x = 1, 2, 4, 8) over BP, as shown in Fig. 4. Bader charge calculations indicate that as the discharge process proceeds, more and more electrons are transferred

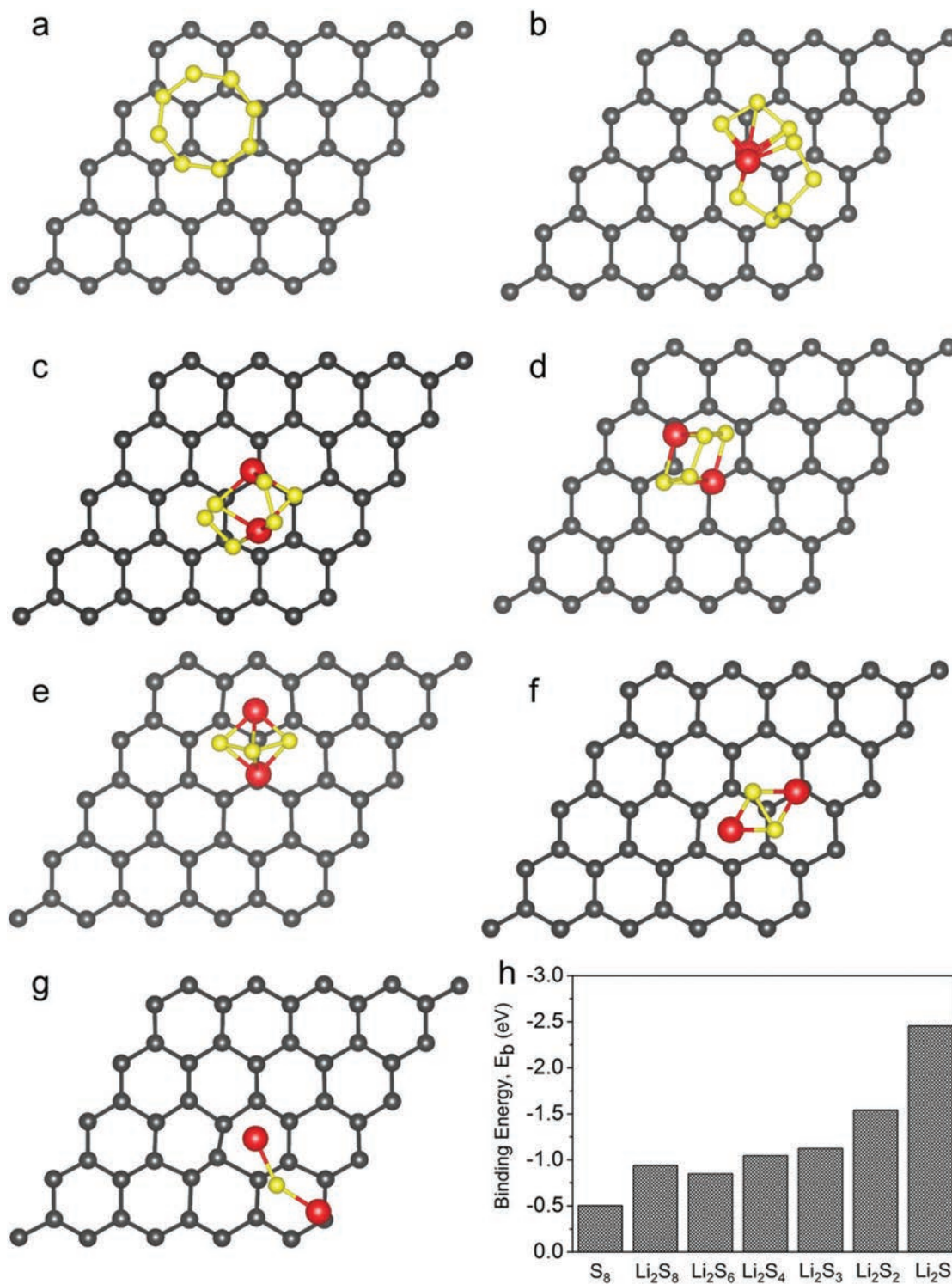


Fig. 3 The most favorable adsorption sites of (a) Li_2S , (b) Li_2S_2 , (c) Li_2S_3 , (d) Li_2S_4 , (e) Li_2S_6 , (f) Li_2S_8 and (g) S_8 systems over monolayer pristine blue phosphorene. (h) Binding energy of all the species on pristine blue phosphorene.

from the LiPSs to the host material. For example, while for the Li_2S_8 molecule the charge gained by BP is $0.01|e|$, for Li_2S_4 , Li_2S_2 and Li_2S molecules the amounts of charge transferred to BP are $0.18|e|$, $0.48|e|$ and $0.66|e|$, respectively. Furthermore,

DCDs of LiPSs for different discharge stages indicate that the electrons donated by the Li atoms are predominantly transferred to the S atoms in the LiPSs owing to the stronger electronegativity of S (2.58) compared to P (2.19). While the P atoms

Table 1 The adsorption energies (E_b), the change in the Li–S bond distance over pristine BP compared to an isolated Li_2S_x molecules ($\Delta_{\text{Li-S}}$), the shortest distance between an Li atom and a P atom in pristine BP ($d_{\text{Li-P}}$), and charge transfer between adsorbates and phosphorene (Q)

	Li_2S_8	Li_2S_6	Li_2S_4	Li_2S_3	Li_2S_2	Li_2S
E_b (eV)	−0.95	−0.86	−1.07	−1.16	−1.54	−2.46
$\Delta_{\text{Li-S}}$ (Å)	0.024	0.11	0.03	0.06	0.11	0.34
$d_{\text{Li-P}}$ (Å)	2.82	2.77	2.58	2.67	2.65	2.53
Q (e)	0.01	0.02	0.18	0.40	0.48	0.66

in BP located close to the LiPSs mostly gain charge, the P atoms in the furrows lose charge to the S atoms. In large LiPSs (see Fig. 4c and d), the S atoms located away from the BP–LiPS interface gain a smaller amount of charge compared to those close to BP.

Similar to pristine BP, a medley of translational and rotational configurations of the LiPSs were considered to find their most energetically stable adsorption sites on BP containing one SV. Unlike pristine BP for which four structurally symmetric sites were considered (see Fig. 1a), for SVBP, the LiPSs were initially located at a distance of 3 Å above the surface in the vicinity of the defective site and were allowed to relax. The most stable adsorption configurations of all the LiPSs and the corresponding magnitudes of E_b are presented in Fig. 5, with the strongest adsorption energy for each Li_2S_x molecule being −2.11 eV for Li_2S_8 , −1.4 eV for Li_2S_6 , −3.13 eV for Li_2S_4 , −2.79 eV for Li_2S_3 , −3.27 eV for Li_2S_2 , and −4.34 eV for Li_2S . These adsorption energies are significantly larger than those for pristine BP. While the adsorption energies of Li_2S_8 , Li_2S_4 , Li_2S_3 and Li_2S_2 increased by more than 100% (124% for Li_2S_8 , 200% for Li_2S_4 , 148% for Li_2S_3 and 110% for Li_2S_2), those for Li_2S_6 and Li_2S increased by 65% for Li_2S_8 and 76% for Li_2S .

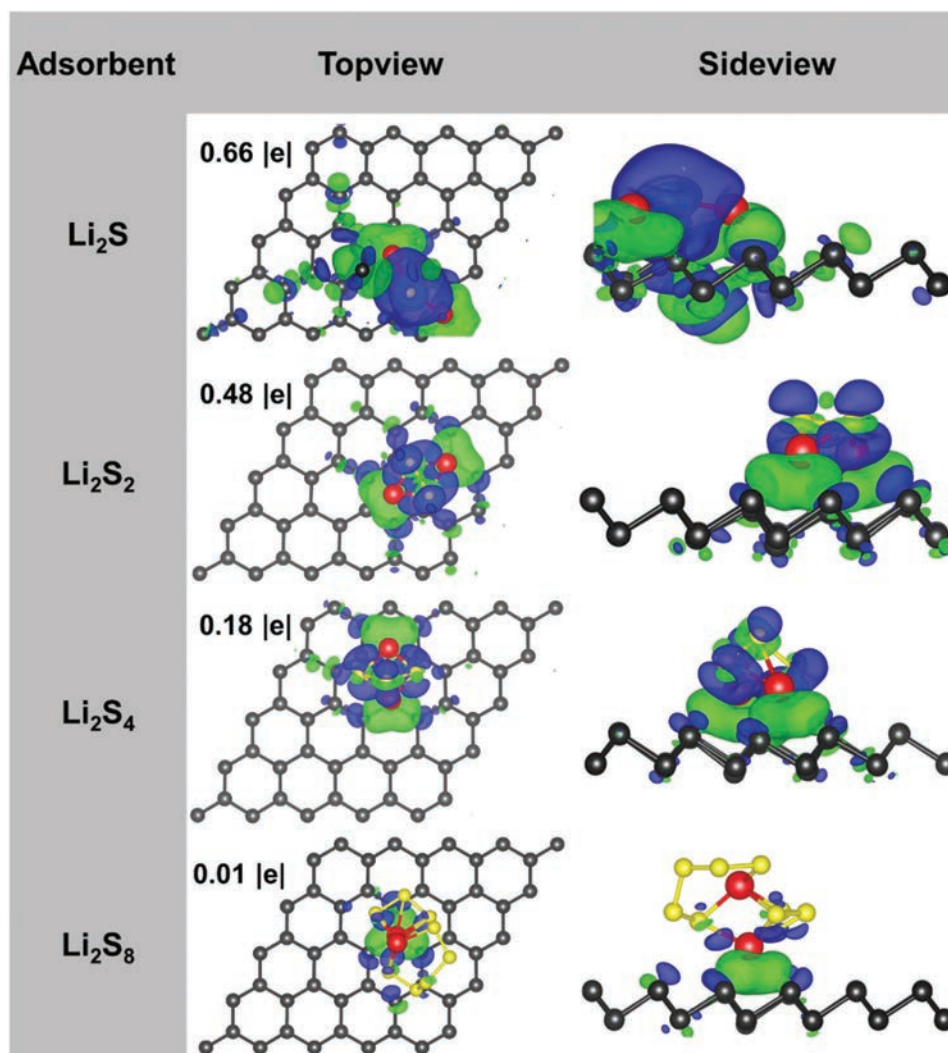


Fig. 4 Differential charge density (DCD) between Li_2S , Li_2S_2 , Li_2S_4 , Li_2S_8 and a pristine BP surface, with top and side views. Color code for atoms: black: P; red: Li; yellow: S. The isosurface level is set at $0.0015 \text{ e} \text{ \AA}^{-3}$. The blue and green regions indicate charge accumulation and depletion, respectively. Bader charge numbers indicate the magnitudes of electrons transferred from the LiPSs to the host material.

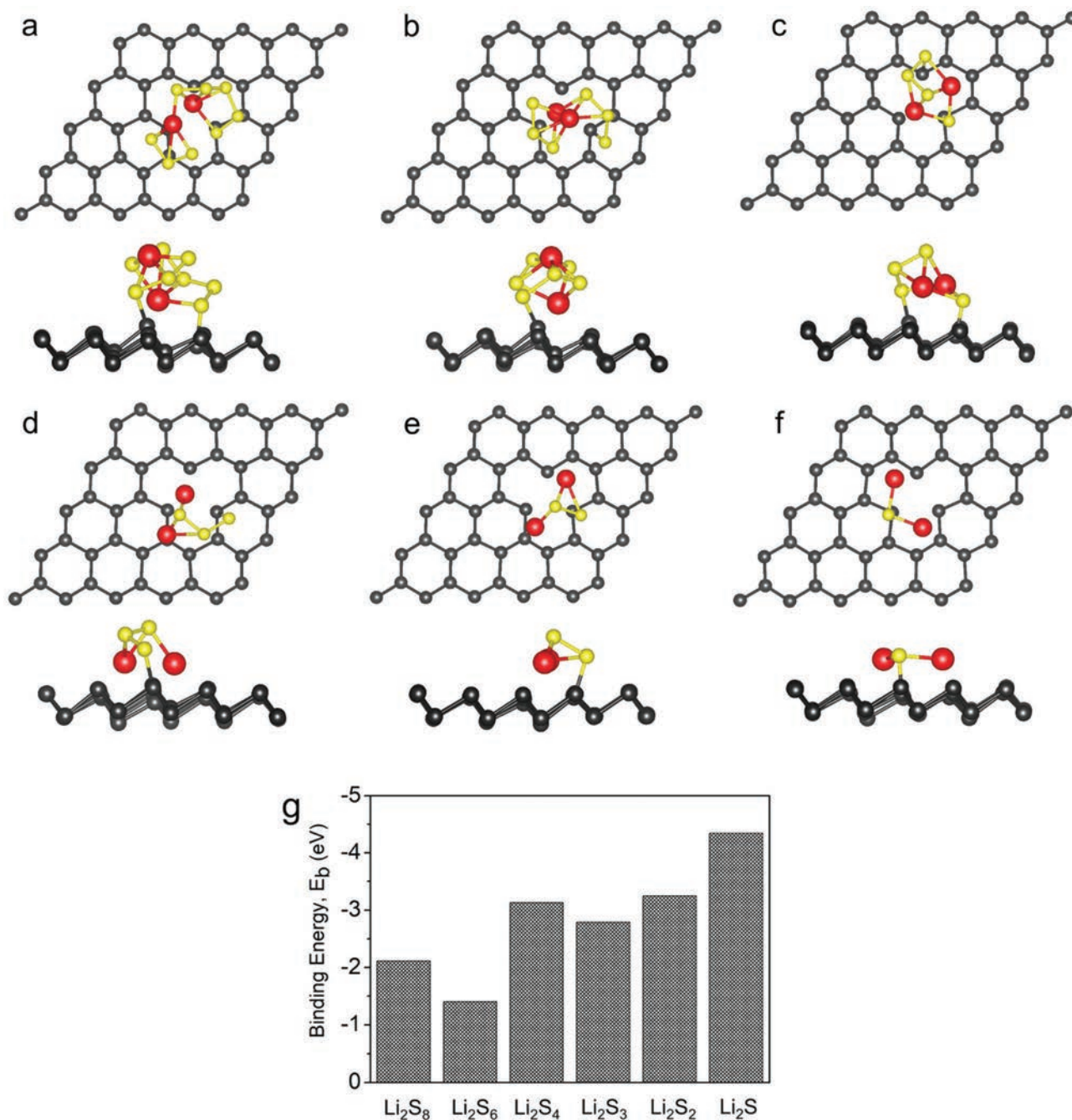


Fig. 5 The most favorable adsorption sites of (a) Li_2S , (b) Li_2S_2 , (c) Li_2S_3 , (d) Li_2S_4 , (e) Li_2S_6 and (f) Li_2S_8 over monolayer defective blue phosphorene. (g) Binding energy of all the species on defective blue phosphorene.

It can be seen that the LiPSs are pulled towards the defective site, indicating that the defects act as traps for the LiPSs in a similar manner to the behavior of defective graphene³¹ and borophene.⁴⁸ Previous studies have reported that increased adsorption energies of LiPSs on 2D hosts come at the cost of irreversible structural distortions,⁴⁹ which can lead to the dissolution of sulfur. For example, Jand *et al.*³¹ reported that point defects in graphene deform the LiPSs, so much so that S atoms detach from the molecules and get adsorbed in the

point defect. Such a behavior was attributed to the strong interactions caused by the localized levels of dangling bonds in under-coordinated C atoms neighboring the vacancy.⁵⁰ Similarly, large adsorption energies caused by strong interactions between striped borophene and polysulfides lead to the decomposition of the adsorbents.⁴⁸ In defective BP however, P-P bonds are not broken during the entire reaction, which implies structural stability of the host. The increase in the Li-S bond lengths after binding to defective BP was larger

compared to pristine BP. For instance, $\Delta_{\text{Li-S}}$ for Li_2S_8 , Li_2S_6 , Li_2S_3 , Li_2S_2 and Li_2S was found to be 0.037 Å, 0.033 Å, 0.011 Å and 0.021 Å, respectively. In addition, the larger soluble LiPS molecules also remain intact over defective BP maintaining their ring-like structures. DCDs shown in Fig. 6 qualitatively show that the interaction between LiPSs and defective BP is much stronger compared to pristine BP. Charge donated by Li atoms is shared by both S atoms and the defective BP substrate. Interestingly, Bader charge calculations indicated that unlike pristine BP, charge is transferred from the substrate to the larger polysulfides while the smaller polysulfides donate charge to the substrate. Specifically, defective BP accepted electrons amounting to 0.738|e|, 0.737|e|, and 0.717|e| from Li_2S , Li_2S_2 and Li_2S_3 , respectively, and larger polysulfides such as

Li_2S_4 , Li_2S_6 and Li_2S_8 accepted 1.12|e|, 0.02|e|, and 0.12|e| from BP.

The stability of the LiPSs over pristine and SV blue phosphorene surfaces at 300 K was studied using AIMD simulations to account for thermal effects. These thermodynamic stabilities were assessed by plotting the time-traces of temperature and total energies (Fig. S1 and S2†) and ensuring that no major deviations from equilibrium occurred. The dynamic evolution of the systems is visualized in ESI Movie 1–12.† It can be seen from these video files that structural distortions to the LiPSs were larger on pristine BP compared to those when an SV is present. Over pristine BP, the Li atoms predominantly hop over the C and P sites. Additionally, the LiPSs frequently migrate to the neighboring hexagonal units, maintaining their

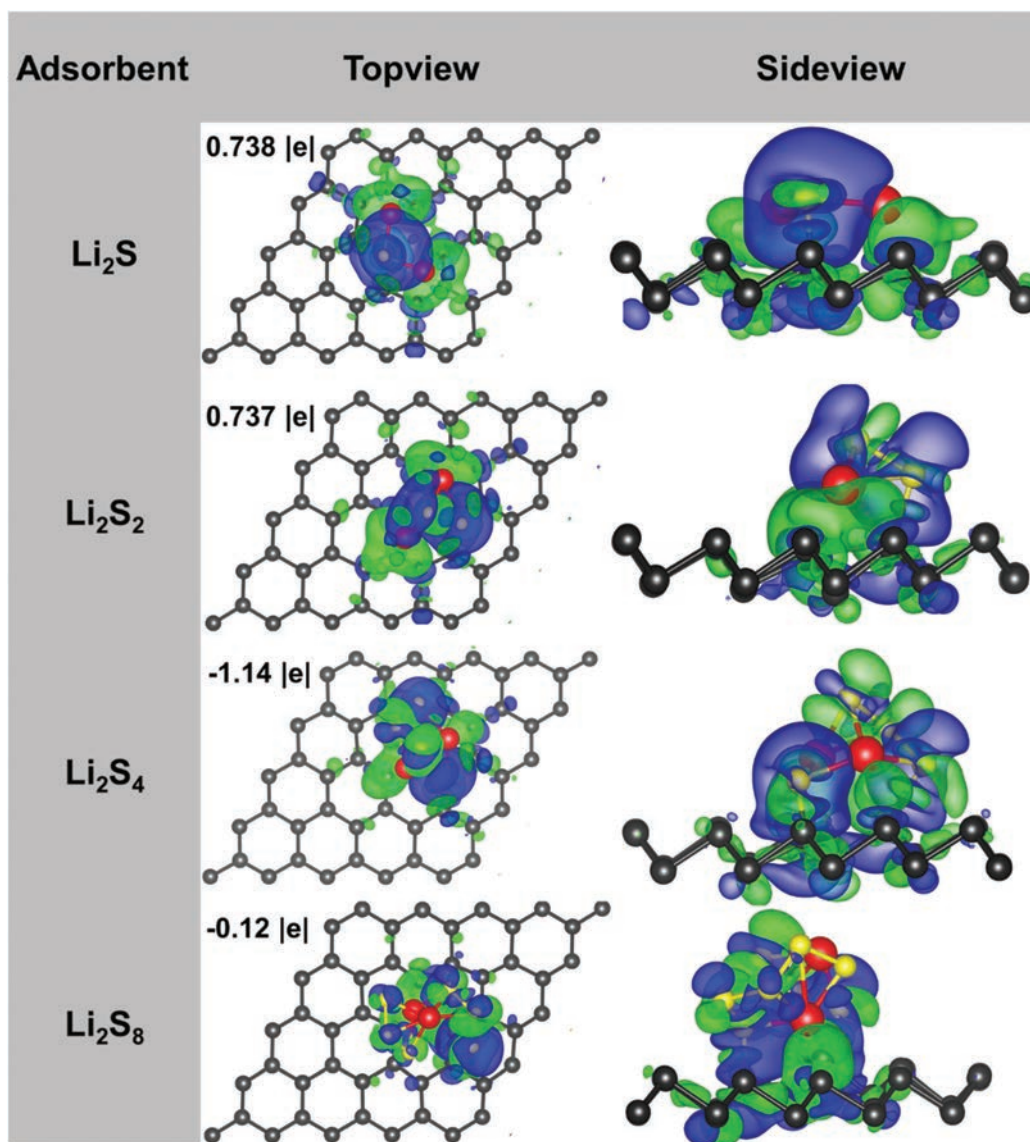


Fig. 6 Differential charge density (DCD) between Li_2S , Li_2S_2 , Li_2S_4 , Li_2S_8 and a defective BP surface, with top and side views. Color code for atoms: black: P; red: Li; yellow: S. The isosurface level is set at $0.0015 \text{ e} \text{ \AA}^{-3}$. The blue and green regions indicate charge accumulation and depletion, respectively. Bader charge numbers indicate the magnitudes of electrons transferred from the LiPSs to the host material.

structural shape. Furthermore, the rotational and translational motions of the larger LiPSs were found to be less pronounced than those of the smaller LiPSs. Comparatively, the defective site in SVBP acts as an entrapment for the Li atoms and the LiPSs are stuck to the substrate. This is further evidenced from the greater restriction in their movement relative to the pristine case, thereby signaling increased trapping behavior *via* the defects' presence.

In order to assess the relative strengths of chemical and van der Waals interaction, the ratio of vdw interactions (R) was calculated, which is given by $R = (E_b^{vdw} - E_b^{novdw})/E_b^{vdw}$. Here, E_b^{vdw} and E_b^{novdw} represent the adsorption energies of LiPSs with and without vdw interactions. The magnitudes of R for LiPSs over pristine and defective BP are shown in Fig. 7. The following observations can be made from the values of R : (a) the strength of vdw interaction is stronger in pristine BP compared to defective BP. Therefore, the chemical interaction of LiPSs over BP is stronger in defective BP than that in pristine BP during the entire discharge process. (b) The weight of R for different LiPSs is different for both pristine and defective BP. (c) For the smaller LiPSs, formed during the end of the lithiation, chemical interaction is the dominant mechanism. Given this context, vdw interactions, which are often ignored,^{12,47,51–53} should be considered for adsorption and diffusion of LiPSs over 2D substrates for accuracy and more effective screening.

Electronic properties of blue phosphorene with bound Li_2S_x species

Li-S batteries composed of pure S_8 as the cathode suffer from poor electrical conductivities due to the low electronic conductivity of elemental sulfur ($5 \times 10^{-30} \text{ S cm}^{-1}$ at 25°C).⁵⁴ To investigate the influence of SVs on the electronic properties during discharge, PDOS plots were generated for both pristine and defective substrates. We will first consider the pristine case to provide a reference point for later discussions on the SV's role. As previously discussed, polysulfide chains with

higher sulfur concentrations are soluble whereas lower concentration chains are insoluble. As representatives for each stage of the process, Li_2S_2 and Li_2S_4 are selected to represent the insoluble and soluble chains, respectively.

In the pristine case, both sample polysulfides demonstrate the formation of islands of states within the band gap (Fig. 8(a and b)). These islands stem mainly from the p-orbitals of sulfur, with minor contributions from phosphorus s and p-orbitals. In addition to these islands, sulfur donates states to both the valence band and the conduction band. Some hybridization is observed in the valence band of Li_2S_2 and the conduction band of Li_2S_4 between S-p and P-s states, indicating covalent bonding character. Interestingly, an island forms with the Fermi level at its maximum, which draws comparison with that of defective BP before adsorption. Most importantly, the new band gap from the maximum of this island to the conduction band is significantly reduced relative to that before adsorption. Therefore, in the pristine case, the polysulfide chains are predicted to increase the conductivity of the system relative to that before adsorption.

Turning our attention to the electronic influence of polysulfides on defective BP, hybridization can again be observed between the p-orbitals of sulfur and phosphorus in both Li_2S_2 and Li_2S_4 (Fig. 5(c and d)). Like the PDOS of defective BP without adatoms, there exists an island of states at the Fermi level for both soluble and insoluble polysulphides. With Li_2S_2 adsorbed, the Fermi level sits in the middle of the island at the Fermi level, implying metallic behaviour.

The conclusion that may be drawn from comparing the electronic behaviour of both pristine and defective BP undergoing discharge in the battery is that while pristine BP is anticipated to demonstrate increased conductivity, defective BP is superior through its predicted metallic character. Put differently, the introduction of an SV should be beneficial considering its electronic properties.

Diffusion of Li and LiPSs across BP

Previous research carried out by Cui and coworkers demonstrated the importance of the diffusion of LiPSs in the cathode material for suppressing the shuttle effect, achieving maximal capacity and overall improvement in the performance of Li-S batteries.⁵¹ Additionally, fast diffusion of Li atoms over the cathode surface results in higher deposition efficiency, and therefore, determines the distribution and growth of Li_2S . On the other hand, poor reaction rates arising from large energy barriers could result in electrochemically inactive large agglomerates of Li_2S over the cathode material, leading to capacity fading. Still, while assessing the suitability of 2D materials as cathodes in Li-S batteries, the diffusivity aspect is often ignored due to the associated computational cost. Here, to assess pristine BP's performance in this regard, the diffusion of an isolated Li atom is considered along both the armchair and zigzag directions.

The diffusion of Li atoms is pivotal to the overall performance of the battery; a cathode material with a small diffusion barrier could potentially propel the redox reactions and encour-

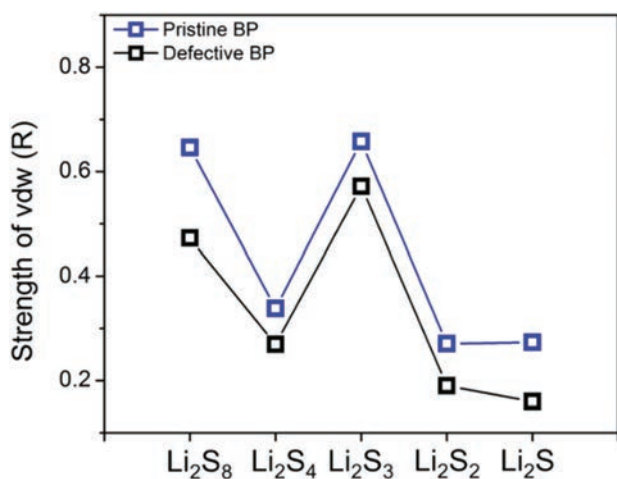


Fig. 7 Strength of van der Waals interactions of LiPS over pristine and defective BP.

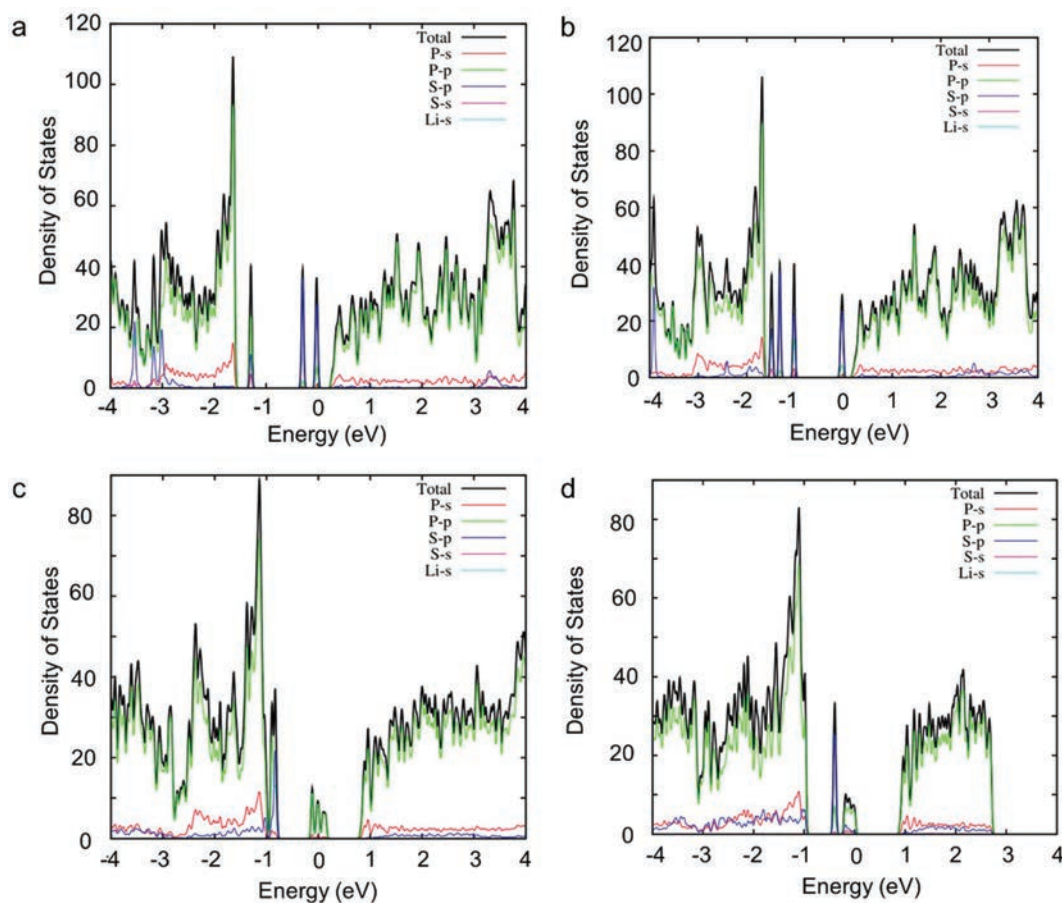


Fig. 8 PDOS of (a) Li₂S₂ and (b) Li₂S₄ adsorbed over pristine BP. PDOS of (c) Li₂S₂ and (d) Li₂S₄ adsorbed over defective BP.

rage sulfur utilization at the surface. Zhou *et al.* showed that the peak-current profile during first and second cathodic reduction processes in metal–sulfide based Li–S correlates strongly with the energy barrier associated with the diffusion barrier of Li.⁵⁵ The P-site is the most favored site for a Li atom with a binding energy of -0.64 eV. Therefore, as shown in Fig. 9(a), the minimum energy paths (MEP) for Li diffusion are: (a) path P → C → R → B → P along the armchair direction and (b) path P → P along the zigzag direction. The energy profiles associated with these MEPs are shown in Fig. 9(b). For the path P → C → R → B → P, the migration barriers (ΔE) are 0.45 and 0.1 eV, respectively. The larger barrier of 0.45 eV is required to migrate over an R site approaching from a C-site. However, diffusion from one R-site to the next P-site, at the beginning of this path, requires a smaller barrier of 0.1 eV. Therefore, the R-site is the transition state for diffusion of Li atoms in the armchair direction. On the other hand, for diffusion in the zigzag direction, the energy barrier is significantly smaller, only 0.12 eV. In the zigzag direction, the transition state is located at the center of the P → P path. The diffusional characteristics of Li over pristine BP are similar to those of Na and K.⁴⁶ A comparison of energy barriers for the diffusion of Li, Na and K over BP is presented in Table S1.† It is interesting to note that energy barriers for different alkali

metals (Li, Na, K) decrease with increasing atomic radius. According to the Arrhenius equation, the diffusion constant (D) is given by

$$D = \nu \exp\left(-\frac{E_A}{k_B T}\right) \quad (5)$$

in which k_B is the Boltzmann constant, T is the operating temperature and ν is a prefactor which depends on the zero-point energy and entropic effects. Using eqn (5), at 300 K, the diffusion of Li in the zigzag direction is 3.5×10^5 times faster than that in the armchair direction assuming that the prefactor is comparable in both the directions (which could be addressed in future studies). This behavior is similar to black phosphorene,⁵⁶ β_{12} -borophene,⁵⁷ and χ_3 -borophene⁵⁷ but dissimilar to striped borophene.^{58,59} To assess the diffusional characteristics of LiPSs, NEB calculations were performed for the large LiPSs, which are the most abundant large LiPSs formed during discharge, *i.e.*, Li₂S₈, Li₂S₆ and Li₂S₄.^{60,61} From a thermodynamic viewpoint, during discharge, the large LiPSs would diffuse from the most favored adsorption site to a neighboring site in the armchair and zigzag directions. The MEPs and their associated energy profiles for the diffusion of LiPSs are shown in Fig. 9(c–h). The migration barriers for the

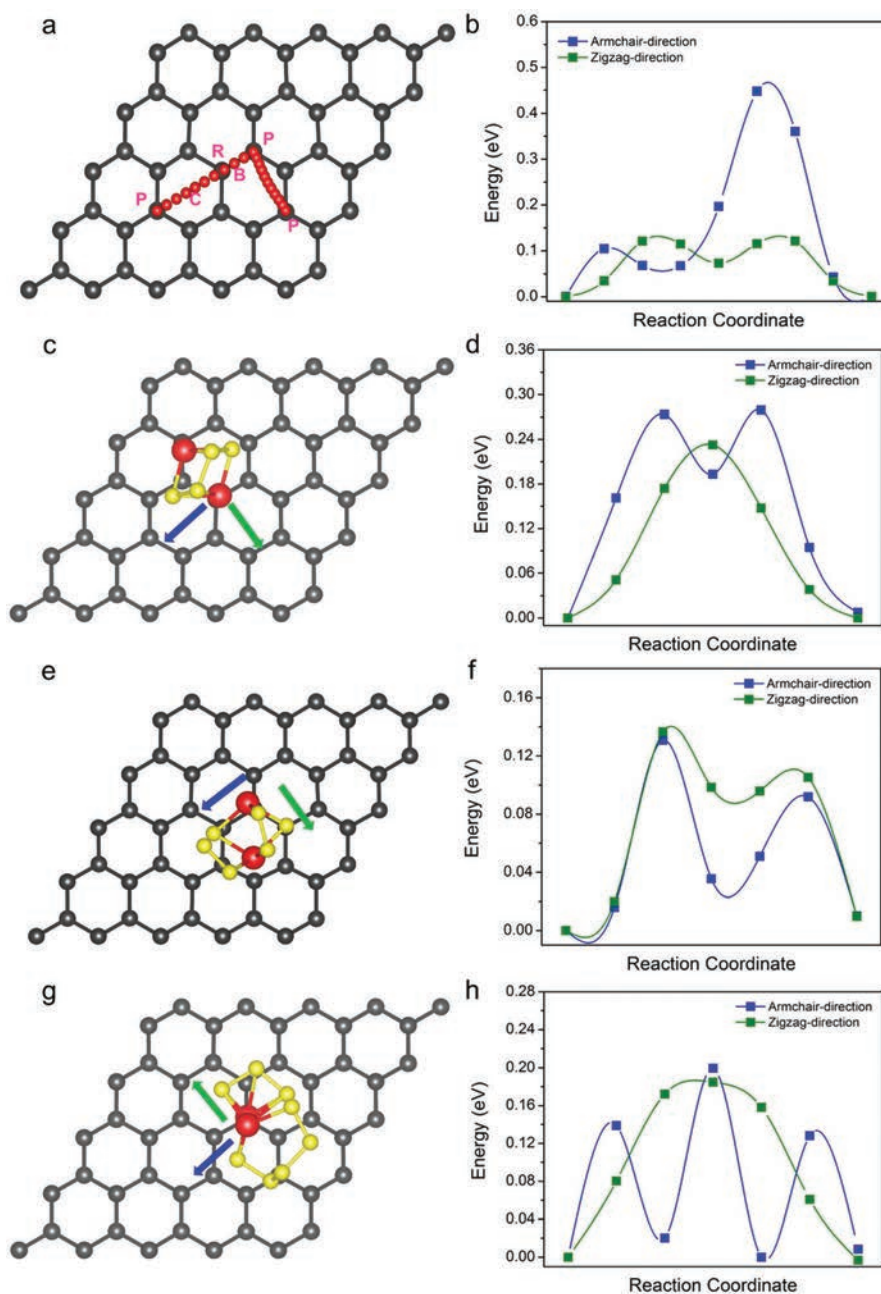


Fig. 9 Minimum energy pathways and their associated energy profiles for (a, b) a Li atom, (c, d) a Li₂S₄ molecule, (e, f) a Li₂S₆ molecule, and (g, h) a Li₂S₈ molecule over a pristine BP surface in the armchair and zigzag directions, initiating at their most-favored adsorption site, and concluding at a symmetrically comparable site in the neighboring primitive cell.

LiPSs along the armchair-direction are 0.28 eV, 0.13 eV, and 0.2 eV for Li₂S₄, Li₂S₆, and Li₂S₈, respectively. It's worth noting that the barriers to diffusion in the zigzag direction are smaller, with diffusion barriers of 0.23 eV, 0.13 eV, and 0.18 eV, respectively. This behavior is similar to black phosphorene and dissimilar to β_{12} -borophene. Furthermore, for Li₂S₄, during diffusion, two Li–P bonds are broken and recreated, which could lead to the largest energy barrier. Overall, these energy barriers which are among the smallest reported could enable ultrafast diffusion of LiPSs. Using TiO₂/TiN decorated

graphene for reference, the energy barrier associated with Li₂S₄ diffusion is 1.04 eV.⁶² For β_{12} -borophene, the energy barriers are 0.99 eV and 0.61 eV for Li₂S₄ and Li₂S₆, respectively.⁶³ Moreover, while the energy barriers for LiPSs' migration over BP in the zigzag direction are comparable to those with black phosphorene, those in the armchair direction are significantly smaller.⁴² Therefore, according to eqn (5) the diffusion of Li₂S_x ($x = 4, 6, 8$) over BP is almost isotropic (unlike the diffusion of a Li atom), with the ratio of diffusivities in the zigzag and armchair directions being 6.9 at 300 K (assuming comparable pre-

factors). While slower diffusion resulting from larger barriers in the armchair direction could lead to clustering of LiPSs over black phosphorene, such a problem would not arise in pristine BP due to similar values of diffusivities in both the armchair and zigzag directions. Therefore, these modest migration barriers will allow for ultrafast transfer of Li_2S_4 , Li_2S_6 and Li_2S_8 over the cathode material, thereby suppressing the agglomeration of LiPSs.

Additionally, we studied the effect of SV on the energy barriers associated with the migration of LiPSs. Overall, the NEB results indicate that the energy barriers increase over SV containing BP compared to pristine BP. The MEPs and their associated energy profiles are shown in Fig. 10(a–d). This behavior is similar to the migration of Li atoms over defective graphene⁶⁴ and black phosphorene⁶⁵ as well as Li and Na diffusion over monolayer ReS_2 .⁶⁶ For example, the energy barrier for the migration of Li_2S_4 was found to be 0.58 eV over SV containing BP as opposed to a barrier of 0.28 eV over pristine BP. Similarly, for the Li_2S_8 molecule the barrier increased to 0.59 eV in contrast to 0.18 eV for pristine BP. These results indicate that the trade-off for increased binding energy from defects is that weakened rate capabilities can arise. Therefore, the selection of an appropriate defect concentration could offer stronger binding from defects and faster rate capabilities from the pristine regions, paving the way for next generation Li–S technologies.

Catalytic decomposition of Li_2S over BP

During the charging process, the final discharge product (Li_2S) decomposes and converts to a S_8 molecule by cleaving the Li–S bond. While redox mediators in the aqueous electrolyte can promote the reaction, the cathode can also help in catalyzing the said reaction, thereby improving the charging efficiency of the cell. In this report, the role of pristine and defective BP in the catalytic oxidation of Li_2S was studied. Recently, Zhou *et al.* demonstrated that the voltage during the first charge cycle in metal–sulfide based Li–S correlates strongly with the energy barrier associated with the decomposition reaction.⁵⁵ CI-NEB simulations were performed to study the energy barrier associated with the reaction: $\text{Li}_2\text{S} \rightarrow \text{LiS} + \text{Li}^+ + \text{e}^-$, *i.e.* the additional energy required to break a Li–S bond and allow a Li atom to diffuse away to its energetically favorable adsorption site (P-site). The MEPs and their associated energy profiles for the decomposition processes on pristine and defective BP are shown in Fig. 11. The breakdown of a Li_2S molecule is determined by the binding strength of Li atoms over BP and the strength of a Li–S bond. The energy required for the above-mentioned reaction is 0.55 eV and 0.50 eV over pristine and defective BP, respectively. In contrast, the binding strength of a Li atom over pristine graphene is weaker⁶⁷ compared to BP, which leads to a significantly larger energy barrier of 1.81 eV.⁵⁵ Furthermore, the energy barriers for the decomposition of Li_2S

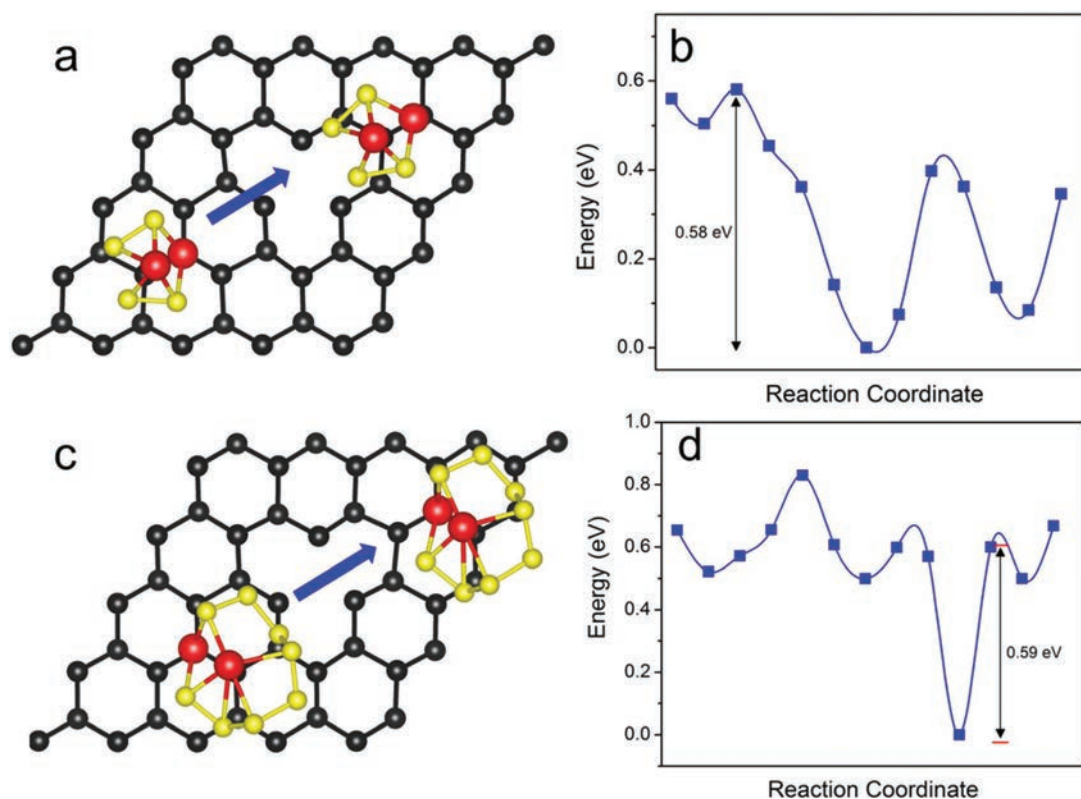


Fig. 10 Minimum energy pathways and their associated energy profiles for (a, b) a Li_2S_4 molecule, and (c, d) a Li_2S_8 , across the SV containing BP surface in the armchair direction, initiating at their most-favored adsorption site and concluding at a symmetrically comparable site in the neighboring primitive cell.

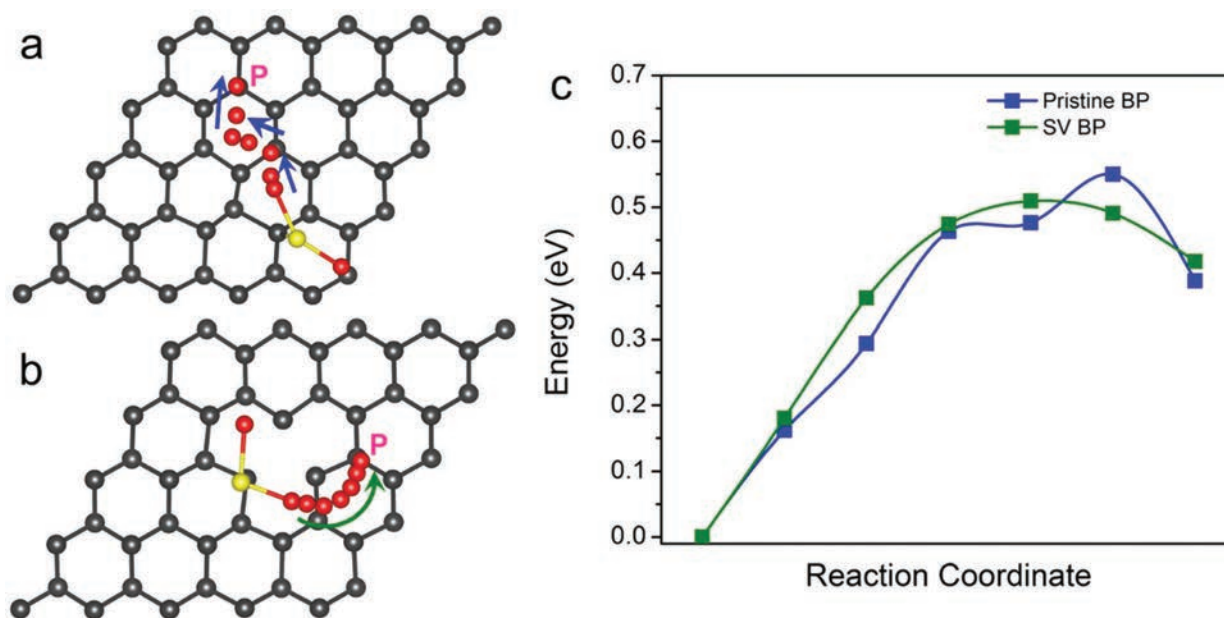


Fig. 11 Minimum energy pathways for the decomposition of a Li–S bond over (a) pristine and (b) defective BP. (c) Their associated energy profiles.

over graphene,⁵⁵ TiCS₂,⁶⁸ FeS,⁵⁵ and CoS₂⁵⁵ are 1.81 eV, 1.51 eV, 0.63 eV and 0.56 eV, respectively, which are larger compared to both pristine and defective BP. Using these energy barriers, the rate constant, k , for the decomposition reaction is given by an Arrhenius type equation: $k = k_0 \exp\left(\frac{-E_A}{k_B T}\right)$, where k_0 is a prefactor, and E_A is the activation barrier. The magnitude of the prefactor depends on the interaction strength between the substrate and the Li₂S molecule and therefore would vary for different systems. Nonetheless, such high energy barriers could reduce the decomposition reaction rate by orders of magnitude due to its exponential dependence on E_A whereas the rate is linearly proportional to k_0 . Moreover, as the interaction between Li and pristine or defective BP is stronger than that with graphene, as shown by its activation barriers, BP substrates can potentially allow for the oxidative decomposition of Li–S bonds at a faster rate.

Application to blue phosphorene based Li–S cathodes

The results presented so far establish that blue phosphorene strategically engineered with single vacancies could inhibit the shuttle effect and help catalyze the oxidative decomposition of Li₂S during the charge process. Li *et al.* synthesized 2D black phosphorene, using a gas-transformation method, which was subsequently mixed with carbon nanofibers to prepare the cathode mix for a Li–S battery.¹⁴ This method helped attain a high volumetric capacity, which is difficult to achieve solely by using 2D materials due to their large surface to volume ratios. Other 2D materials (*e.g.* graphene^{69–72}), transition metal chalcogenides (*e.g.* MoS₂⁷³ and ReS₂¹²), and MXene materials (*e.g.* Ti₂C¹³) were also integrated into the cathode of Li–S batteries to attain high capacities and showed improved cycle life by suppressing the shuttle-effect. Similarly, blue phosphorene

can be incorporated into the cathode mix by preparing 2D blue phosphorene from a bulk black phosphorene crystal, a method proposed by Golias *et al.*⁷⁴ Moreover, several techniques can be used *ex situ* to introduce single vacancies to the blue phosphorene lattice. For example, the electron beam irradiation technique was used to create vacancy defects in graphene⁷⁵ and hexagonal BN.⁷⁶ Thermal annealing,⁷⁷ α -particle bombardment,⁷⁸ and proton beam irradiation⁷⁹ techniques are also alternative methods used to create vacancies in 2D materials. For example, very recently, Huang *et al.* employed a visible-light assisted pre-electrolysis process to introduce defects into ReS₂ nanosheets, which showed enhanced oxygen evolution activity.⁸⁰ Considering these practical examples of implementing 2D materials into batteries and their defect engineering, the beneficial role of defects becomes a grounded possibility for future experimental investigations.

Conclusion

Herein, the adsorption behavior of different lithium polysulfides has been studied over monolayer pristine and defective phosphorene, a recently synthesized 2D material. A meticulous searching scheme was used to find the best adsorption sites for the LiPSs. Results indicated that the adsorption energies for LiPSs over pristine BP are moderate, in the range of -0.86 eV to 2.45 eV. Interestingly, the creation of a single vacancy increased the adsorption energy by up to 200%, with the strongest adsorption energies being -2.11 eV, -1.4 eV, -3.13 eV, -2.79 eV, 3.25 eV, and 4.34 eV for Li₂S₈, Li₂S₆, Li₂S₄, Li₂S₃, Li₂S₂, and Li₂S, respectively. Furthermore, increased adsorption energies did not cause any significant structural deformation of the reactants, which is essential in avoiding capacity

fading. Bader charge analysis, differential charge density analysis and projected density of state calculations were carried out to understand the underlying mechanisms of adsorption of different LiPSs over BP substrates. From the PDOS plots, we observed that pristine BP undergoes an improvement of conductivity during the discharge process, but the metallic behaviour of defective BP makes it superior in this regard. Finally, climbing-image nudged elastic band simulations were carried out to search for the minimum energy paths and energy barrier profiles associated with both the diffusion of Li ions and large soluble LiPSs over pristine BP. The energy barrier for the migration of Li was found to be anisotropic, with the barrier in the zigzag direction three times smaller than that in the armchair direction. Furthermore, the migration barriers of the LiPSs were found to be very small and of similar magnitudes in both the armchair and zigzag directions, with the lowest diffusion energy barriers being 0.23 eV, 0.13 eV and 0.18 eV for Li₂S₄, Li₂S₆ and Li₂S₈, respectively. These ultra-small energy barriers in both the in-plane directions would help in the conversion of adsorbed large LiPSs. To summarize, the insights obtained from this study motivate defect-engineering monolayer BP for its use as a cathode in Li-S batteries. In future, the remaining phosphorene polymorphs and other 2D materials should be screened for Li-S batteries to effectively explore their unique structural and electronic properties for tunable electrode properties.

Author contributions

All of the authors contributed towards the preparation of the manuscript and have given approval to the current version.

Conflicts of interest

There are no conflicts to declare.

Acknowledgements

The authors acknowledge funding from the Natural Sciences and Engineering Research Council of Canada (NSERC) through the Discovery grant, and undergraduate scholarship programs, the Hart professorship, and the University of Toronto. We also acknowledge Compute Canada for providing computing resources at the SciNet CalculQuebec, and Westgrid consortia. The authors also thank Prof. Nikhil Koratkar and Mr Sean Grixti for important discussions.

References

- Q. Pang, X. Liang, C. Y. Kwok and L. F. Nazar, Advances in lithium-sulfur batteries based on multifunctional cathodes and electrolytes, *Nat. Energy*, 2016, **1**(9), 16132.
- L. Ma, K. E. Hendrickson, S. Wei and L. A. Archer, Nanomaterials: Science and applications in the lithium-sulfur battery, *Nano Today*, 2015, **10**(3), 315-338.
- P. E. Blöchl, Projector augmented-wave method, *Phys. Rev. B: Condens. Matter Mater. Phys.*, 1994, **50**(24), 17953.
- R. Service, Lithium-sulfur batteries poised for leap, *Science*, 2018, **359**(6380), 1080.
- A. Manthiram, Y. Fu, S.-H. Chung, C. Zu and Y.-S. Su, Rechargeable lithium-sulfur batteries, *Chem. Rev.*, 2014, **114**(23), 11751-11787.
- Y. M. Lee, N.-S. Choi, J. H. Park and J.-K. Park, Electrochemical performance of lithium/sulfur batteries with protected Li anodes, *J. Power Sources*, 2003, **119**, 964-972.
- C.-W. Lee, Q. Pang, S. Ha, L. Cheng, S.-D. Han, K. R. Zavadil, K. G. Gallagher, L. F. Nazar and M. Balasubramanian, Directing the lithium-sulfur reaction pathway via sparingly solvating electrolytes for high energy density batteries, *ACS Cent. Sci.*, 2017, **3**(6), 605-613.
- D.-c. Rezan, *Li-S Batteries: The Challenges, Chemistry, Materials, and Future Perspectives*, # N/A, 2017.
- Q. Zhang, Y. Wang, Z. W. Seh, Z. Fu, R. Zhang and Y. Cui, Understanding the anchoring effect of two-dimensional layered materials for lithium-sulfur batteries, *Nano Lett.*, 2015, **15**(6), 3780-3786.
- D. Liu, C. Zhang, G. Zhou, W. Lv, G. Ling, L. Zhi and Q. H. Yang, Catalytic effects in lithium-sulfur batteries: promoted sulfur transformation and reduced shuttle effect, *Adv. Sci.*, 2018, **5**, 1700270.
- G. Zhou, L. Li, C. Ma, S. Wang, Y. Shi, N. Koratkar, W. Ren, F. Li and H.-M. Cheng, A graphene foam electrode with high sulfur loading for flexible and high energy Li-S batteries, *Nano Energy*, 2015, **11**, 356-365.
- J. Gao, L. Li, J. Tan, H. Sun, B. Li, J. C. Idrobo, C. V. Singh, T.-M. Lu and N. Koratkar, Vertically Oriented Arrays of ReS₂ Nanosheets for Electrochemical Energy Storage and Electrocatalysis, *Nano Lett.*, 2016, **16**(6), 3780-3787.
- X. Liang, Y. Rangom, C. Y. Kwok, Q. Pang and L. F. Nazar, Interwoven MXene Nanosheet/Carbon-Nanotube Composites as Li-S Cathode Hosts, *Adv. Mater.*, 2017, **29**(3), 1603040.
- L. Li, L. Chen, S. Mukherjee, J. Gao, H. Sun, Z. Liu, X. Ma, T. Gupta, C. V. Singh and W. Ren, Phosphorene as a Polysulfide Immobilizer and Catalyst in High-Performance Lithium-Sulfur Batteries, *Adv. Mater.*, 2017, **29**(2), 1602734.
- Y. Zheng, H. Li, H. Yuan, H. Fan, W. Li and J. Zhang, Understanding the anchoring effect of Graphene, BN, C 2 N and C 3 N 4 monolayers for lithium-polysulfides in Li-S batteries, *Appl. Surf. Sci.*, 2018, **434**, 596-603.
- J. Wu and L.-W. Wang, 2D frameworks C 2 N as a potential cathode for lithium sulfur batteries: an ab initio density functional study, *J. Mater. Chem. A*, 2018, **6**(7), 2984-2994.
- S. Li, S. Yang, D. Shen, W. Sun, X. Shan, W. Dong, Y. Chen, X. Zhang, Y. Mao and S. Tang, Polysulfide intercalation in bilayer-structured graphitic C 3 N 4: a first-principles study, *Phys. Chem. Chem. Phys.*, 2017, **19**(48), 32708-32714.

- 18 S. Grixti, S. Mukherjee and C. V. Singh, Two-dimensional boron as an impressive lithium-sulphur battery cathode material, *Energy Storage Mater.*, 2018, **13**, 80–87.
- 19 Z. Liu, P. B. Balbuena and P. P. Mukherjee, Evaluating silicene as a potential cathode host to immobilize polysulfides in lithium-sulfur batteries, *J. Coord. Chem.*, 2016, **69**(11–13), 2090–2105.
- 20 Z. Zhu and D. Tománek, Semiconducting layered blue phosphorus: a computational study, *Phys. Rev. Lett.*, 2014, **112**(17), 176802.
- 21 J. Zeng, P. Cui and Z. Zhang, Half layer by half layer growth of a blue phosphorene monolayer on a GaN(001) substrate, *Phys. Rev. Lett.*, 2017, **118**(4), 046101.
- 22 J. L. Zhang, S. Zhao, C. Han, Z. Wang, S. Zhong, S. Sun, R. Guo, X. Zhou, C. D. Gu and K. D. Yuan, Epitaxial growth of single layer blue phosphorus: a new phase of two-dimensional phosphorus, *Nano Lett.*, 2016, **16**(8), 4903–4908.
- 23 Q.-F. Li, C.-G. Duan, X. Wan and J.-L. Kuo, Theoretical prediction of anode materials in Li-ion batteries on layered black and blue phosphorus, *J. Phys. Chem. C*, 2015, **119**(16), 8662–8670.
- 24 Q. Peng, Z. Wang, B. Sa, B. Wu and Z. Sun, Blue phosphorene/MS₂(M=Nb, Ta) heterostructures as promising flexible anodes for lithium-ion batteries, *ACS Appl. Mater. Interfaces*, 2016, **8**(21), 13449–13457.
- 25 L.-C. Yin, J. Liang, G.-M. Zhou, F. Li, R. Saito and H.-M. Cheng, Understanding the interactions between lithium polysulfides and N-doped graphene using density functional theory calculations, *Nano Energy*, 2016, **25**, 203–210.
- 26 Y. Qiu, W. Li, W. Zhao, G. Li, Y. Hou, M. Liu, L. Zhou, F. Ye, H. Li and Z. Wei, High-rate, ultralong cycle-life lithium/sulfur batteries enabled by nitrogen-doped graphene, *Nano Lett.*, 2014, **14**(8), 4821–4827.
- 27 Z. Wang, Y. Dong, H. Li, Z. Zhao, H. B. Wu, C. Hao, S. Liu, J. Qiu and X. W. D. Lou, Enhancing lithium-sulphur battery performance by strongly binding the discharge products on amino-functionalized reduced graphene oxide, *Nat. Commun.*, 2014, **5**, 5002.
- 28 G. S. Yi, E. S. Sim and Y.-C. Chung, Effect of lithium-trapping on nitrogen-doped graphene as an anchoring material for lithium-sulfur batteries: a density functional theory study, *Phys. Chem. Chem. Phys.*, 2017, **19**(41), 28189–28194.
- 29 D. Rao, Y. Wang, L. Zhang, S. Yao, X. Qian, X. Xi, K. Xiao, K. Deng, X. Shen and R. Lu, Mechanism of polysulfide immobilization on defective graphene sheets with N-substitution, *Carbon*, 2016, **110**, 207–214.
- 30 W. Zhao, P. Chen, P. Tang, Y. Li, J. Wu and W. Duan, Sulfur immobilization and lithium storage on defective graphene: A first-principles study, *Appl. Phys. Lett.*, 2014, **104**(4), 043901.
- 31 S. P. Jand, Y. Chen and P. Kaghazchi, Comparative theoretical study of adsorption of lithium polysulfides(Li₂S_x) on pristine and defective graphene, *J. Power Sources*, 2016, **308**, 166–171.
- 32 H. Jiang, W. Shyy, M. Liu, Y. Ren and T. Zhao, Borophene and defective borophene as potential anchoring materials for lithium-sulfur batteries: a first-principles study, *J. Mater. Chem. A*, 2018, **6**(5), 2107–2114.
- 33 P. Giannozzi, S. Baroni, N. Bonini, M. Calandra, R. Car, C. Cavazzoni, D. Ceresoli, G. L. Chiarotti, M. Cococcioni and I. Dabo, QUANTUM ESPRESSO: a modular and open-source software project for quantum simulations of materials, *J. Phys.: Condens. Matter*, 2009, **21**(39), 395502.
- 34 R. Fletcher, A new approach to variable metric algorithms, *Comput. J.*, 1970, **13**(3), 317–322.
- 35 V. Barone, M. Casarin, D. Forrer, M. Pavone, M. Sambi and A. Vittadini, Role and effective treatment of dispersive forces in materials: Polyethylene and graphite crystals as test cases, *J. Comput. Chem.*, 2009, **30**(6), 934–939.
- 36 W. Tang, E. Sanville and G. Henkelman, A grid-based Bader analysis algorithm without lattice bias, *J. Phys.: Condens. Matter*, 2009, **21**(8), 084204.
- 37 G. Henkelman, B. P. Uberuaga and H. Jónsson, A climbing image nudged elastic band method for finding saddle points and minimum energy paths, *J. Chem. Phys.*, 2000, **113**(22), 9901–9904.
- 38 Y. Ding and Y. Wang, Structural, electronic, and magnetic properties of adatom adsorptions on black and blue phosphorene: a first-principles study, *J. Phys. Chem. C*, 2015, **119**(19), 10610–10622.
- 39 S. Li, Y. Wu, Y. Tu, Y. Wang, T. Jiang, W. Liu and Y. Zhao, Defects in silicene: vacancy clusters, extended line defects, and di-adatoms, *Sci. Rep.*, 2015, **5**, 7881.
- 40 F. Banhart, J. Kotakoski and A. V. Krasheninnikov, Structural Defects in Graphene, *ACS Nano*, 2011, **5**(1), 26–41.
- 41 W. Hu and J. Yang, Defects in phosphorene, *J. Phys. Chem. C*, 2015, **119**(35), 20474–20480.
- 42 J. Zhao, Y. Yang, R. S. Katiyar and Z. Chen, Phosphorene as a promising anchoring material for lithium-sulfur batteries: a computational study, *J. Mater. Chem. A*, 2016, **4**(16), 6124–6130.
- 43 B. Wang, S. M. Alhassan and S. T. Pantelides, Formation of large polysulfide complexes during the lithium-sulfur battery discharge, *Phys. Rev. Appl.*, 2014, **2**(3), 034004.
- 44 Y. Qie, J. Liu, S. Wang, S. Gong and Q. Sun, C3B monolayer as an anchoring material for lithium-sulfur batteries, *Carbon*, 2017, **129**, 38–44.
- 45 Y. Zhao and J. Zhao, Functional group-dependent anchoring effect of titanium carbide-based MXenes for lithium-sulfur batteries: A computational study, *Appl. Surf. Sci.*, 2017, **412**, 591–598.
- 46 S. Mukherjee, L. Kavalsky, and C. V. Singh, Ultrahigh Storage and Fast Diffusion of Na and K in Blue Phosphorene Anodes, *ACS Appl. Mater. Interfaces*, 2018, **10**(10), 8630–8639.
- 47 L. Zhang, P. Liang, H.-b. Shu, X.-l. Man, F. Li, J. Huang, Q.-m. Dong and D.-l. Chao, Borophene as Efficient Sulfur Hosts for Lithium-Sulfur Batteries: Suppressing Shuttle Effect and Improving Conductivity, *J. Phys. Chem. C*, 2017, **121**(29), 15549–15555.

- 48 H. R. Jiang, W. Shyy, M. Liu, Y. X. Ren and T. S. Zhao, Borophene and defective borophene as potential anchoring materials for lithium–sulfur batteries: a first-principles study, *J. Mater. Chem. A*, 2018, **6**(5), 2107–2114.
- 49 X. Yang, L. Zhang, F. Zhang, Y. Huang and Y. Chen, Sulfur-infiltrated graphene-based layered porous carbon cathodes for high-performance lithium–sulfur batteries, *ACS Nano*, 2014, **8**(5), 5208–5215.
- 50 J. M. Carlsson and M. Scheffler, Structural, electronic, and chemical properties of nanoporous carbon, *Phys. Rev. Lett.*, 2006, **96**(4), 046806.
- 51 X. Tao, J. Wang, C. Liu, H. Wang, H. Yao, G. Zheng, Z. W. Seh, Q. Cai, W. Li and G. Zhou, Balancing surface adsorption and diffusion of lithium-polysulfides on non-conductive oxides for lithium–sulfur battery design, *Nat. Commun.*, 2016, **7**, 11203.
- 52 Z. W. Seh, J. H. Yu, W. Li, P.-C. Hsu, H. Wang, Y. Sun, H. Yao, Q. Zhang and Y. Cui, Two-dimensional layered transition metal disulfides for effective encapsulation of high-capacity lithium sulphide cathodes, *Nat. Commun.*, 2014, **5**, 5017.
- 53 G. Li, X. Wang, M. H. Seo, M. Li, L. Ma, Y. Yuan, T. Wu, A. Yu, S. Wang and J. Lu, Chemisorption of polysulfides through redox reactions with organic molecules for lithium–sulfur batteries, *Nat. Commun.*, 2018, **9**(1), 705.
- 54 E. Peled, Y. Sternberg, A. Gorenshtein and Y. Lavi, Lithium-sulfur battery: evaluation of dioxolane-based electrolytes, *J. Electrochem. Soc.*, 1989, **136**(6), 1621–1625.
- 55 G. Zhou, H. Tian, Y. Jin, X. Tao, B. Liu, R. Zhang, Z. W. Seh, D. Zhuo, Y. Liu and J. Sun, Catalytic oxidation of Li₂S on the surface of metal sulfides for Li–S batteries, *Proc. Natl. Acad. Sci. U. S. A.*, 2017, **114**(5), 840–845.
- 56 W. Li, Y. Yang, G. Zhang and Y.-W. Zhang, Ultrafast and directional diffusion of lithium in phosphorene for high-performance lithium-ion battery, *Nano Lett.*, 2015, **15**(3), 1691–1697.
- 57 P. Xiang, X. Chen, W. Zhang, J. Li, B. Xiao, L. Li and K. Deng, Metallic borophene polytypes as lightweight anode materials for non-lithium-ion batteries, *Phys. Chem. Chem. Phys.*, 2017, **19**(36), 24945–24954.
- 58 D. Rao, L. Zhang, Z. Meng, X. Zhang, Y. Wang, G. Qiao, X. Shen, H. Xia, J. Liu and R. Lu, Ultrahigh energy storage and ultrafast ion diffusion in borophene-based anodes for rechargeable metal ion batteries, *J. Mater. Chem. A*, 2017, **5**(5), 2328–2338.
- 59 H. Jiang, Z. Lu, M. Wu, F. Ciucci and T. Zhao, Borophene: a promising anode material offering high specific capacity and high rate capability for lithium-ion batteries, *Nano Energy*, 2016, **23**, 97–104.
- 60 M. Safari, C. Y. Kwok and L. F. Nazar, Transport properties of polysulfide species in lithium–sulfur battery electrolytes: coupling of experiment and theory, *ACS Cent. Sci.*, 2016, **2**(8), 560–568.
- 61 M. Cuisinier, P.-E. Cabelguen, S. Evers, G. He, M. Kolbeck, A. Garsuch, T. Bolin, M. Balasubramanian and L. F. Nazar, Sulfur speciation in Li–S batteries determined by operando X-ray absorption spectroscopy, *J. Phys. Chem. Lett.*, 2013, **4**(19), 3227–3232.
- 62 T. Zhou, W. Lv, J. Li, G. Zhou, Y. Zhao, S. Fan, B. Liu, B. Li, F. Kang and Q.-H. Yang, Twinborn TiO₂–TiN heterostructures enabling smooth trapping–diffusion–conversion of polysulfides towards ultralong life lithium–sulfur batteries, *Energy Environ. Sci.*, 2017, **10**(7), 1694–1703.
- 63 S. Grixti, S. Mukherjee and C. V. Singh, Two-dimensional boron as an impressive lithium-sulphur battery cathode material, *Energy Storage Mater.*, 2018, **13**, 80–87.
- 64 L.-J. Zhou, Z. Hou and L.-M. Wu, First-principles study of lithium adsorption and diffusion on graphene with point defects, *J. Phys. Chem. C*, 2012, **116**(41), 21780–21787.
- 65 R. Zhang, X. Wu and J. Yang, Blockage of ultrafast and directional diffusion of Li atoms on phosphorene with intrinsic defects, *Nanoscale*, 2016, **8**(7), 4001–4006.
- 66 S. Mukherjee, A. Banwait, S. Grixti, N. Koratkar and C. V. Singh, Adsorption and diffusion of lithium and sodium on defective rhenium disulfide: A first principles study, *ACS Appl. Mater. Interfaces*, 2018, **10**(6), 5373–5384.
- 67 D. Datta, J. Li, N. Koratkar and V. B. Shenoy, Enhanced lithiation in defective graphene, *Carbon*, 2014, **80**, 305–310.
- 68 X. Liu, X. Shao, F. Li and M. Zhao, Anchoring effects of S-terminated Ti₂C MXene for lithium-sulfur batteries: A First-Principles Study, *Appl. Surf. Sci.*, 2018, **455**, 522–526.
- 69 F. Wu, J. T. Lee, E. Zhao, B. Zhang and G. Yushin, Graphene–Li₂S–carbon nanocomposite for lithium–sulfur batteries, *ACS Nano*, 2015, **10**(1), 1333–1340.
- 70 G. Tan, R. Xu, Z. Xing, Y. Yuan, J. Lu, J. Wen, C. Liu, L. Ma, C. Zhan and Q. Liu, Burning lithium in CS₂ for high-performing compact Li₂S–graphene nanocapsules for Li–S batteries, *Nat. Energy*, 2017, **2**(7), 17090.
- 71 G. Zhou, L. Li, D. W. Wang, X. y. Shan, S. Pei, F. Li and H. M. Cheng, A flexible sulfur-graphene-polypropylene separator integrated electrode for advanced Li–S batteries, *Adv. Mater.*, 2015, **27**(4), 641–647.
- 72 D. Su, M. Cortie and G. Wang, Fabrication of N-doped Graphene–Carbon Nanotube Hybrids from Prussian Blue for Lithium–Sulfur Batteries, *Adv. Energy Mater.*, 2017, **7**(8), 1602014.
- 73 H. Lin, L. Yang, X. Jiang, G. Li, T. Zhang, Q. Yao, G. W. Zheng and J. Y. Lee, Electrocatalysis of polysulfide conversion by sulfur-deficient MoS₂ nanoflakes for lithium–sulfur batteries, *Energy Environ. Sci.*, 2017, **10**(6), 1476–1486.
- 74 E. Goliias, M. Krivenkov, A. Varykhalov, J. Sánchez-Barriga and O. Rader, Band renormalization of blue phosphorus on Au(111), *arXiv preprint arXiv:1803.08862*, 2018.
- 75 F. Banhart, J. Kotakoski and A. V. Krasheninnikov, Structural defects in graphene, *ACS Nano*, 2010, **5**(1), 26–41.
- 76 L. G. Cançado, A. Jorio, E. M. Ferreira, F. Stavale, C. Achete, R. Capaz, M. Moutinho, A. Lombardo, T. Kulmala and A. Ferrari, Quantifying defects in graphene via Raman spectroscopy at different excitation energies, *Nano Lett.*, 2011, **11**(8), 3190–3196.

- 77 X. Wei, Z. Yu, F. Hu, Y. Cheng, L. Yu, X. Wang, M. Xiao, J. Wang, X. Wang and Y. Shi, Mo-O bond doping and related-defect assisted enhancement of photoluminescence in monolayer MoS₂, *AIP Adv.*, 2014, **4**(12), 123004.
- 78 S. Tongay, J. Suh, C. Ataca, W. Fan, A. Luce, J. S. Kang, J. Liu, C. Ko, R. Raghunathanan and J. Zhou, Defects activated photoluminescence in two-dimensional semiconductors: interplay between bound, charged, and free excitons, *Sci. Rep.*, 2013, **3**, 2657.
- 79 T.-Y. Kim, K. Cho, W. Park, J. Park, Y. Song, S. Hong, W.-K. Hong and T. Lee, Irradiation effects of high-energy proton beams on MoS₂ field effect transistors, *ACS Nano*, 2014, **8**(3), 2774–2781.
- 80 J. Huang, H. Gao, Y. Xia, Y. Sun, J. Xiong, Y. Li, S. Cong, J. Guo, S. Du and G. Zou, Enhanced photoelectrochemical performance of defect-rich ReS₂ nanosheets in visible-light assisted hydrogen generation, *Nano Energy*, 2018, **46**, 305–313.